Prediction of Binding Affinities for TIBO Inhibitors of HIV-1 Reverse Transcriptase Using Monte Carlo Simulations in a Linear Response Method

Richard H. Smith, Jr.,*[,‡,†] William L. Jorgensen,[§] Julian Tirado-Rives,[§] Michelle L. Lamb,[§] Paul A. J. Janssen,[▽] Christopher J. Michejda,[†] and Marilyn B. Kroeger Smith[†]

Department of Chemistry, Western Maryland College, Westminster, Maryland 21157, ABL-Basic Research Program, NCI−Frederick Research and Development Center, P.O. Box B, Frederick, Maryland 21702-1201, Department of Chemistry, Yale University, New Haven, Connecticut 06520-8107, and Janssen Research Foundation, CMD, Antwerpsesteenweg 37, B-2350 Vosselaar, Belgium

Received July 14, 1998

Monte Carlo (MC) simulations in combination with a linear response approach were used to estimate the free energies of binding for a series of 12 TIBO nonnucleoside inhibitors of HIV-1 reverse transcriptase. Separate correlations were made for the R^6 and S^6 absolute conformations of the inhibitors, as well as for the analogous N6-monoprotonated species. Models based upon the neutral unbound inhibitors produced overall better fits to experimental values than did those using the protonated unbound inhibitors, with only slight differences between the neutral R^6 and S^6 cases. The best results were obtained with a three-parameter linear response equation containing van der Waals (α), electrostatic (β), and solvent accessible surface area (SASA, γ) terms. The averaged (R^6 and S^6) rms error was approximately 0.88 kcal/mol for the observed range of 4.06 kcal/mol in inhibitor activities. The averaged values of α, β, and γ were −0.150, 0.114, and 0.0286, respectively. Omission of the α term gave β 0.152 and γ 0.022 with a rms of 0.92. The unweighted van der Waals components were found to be highly attractive but failed to correlate well across the series of inhibitors. Contrastingly, while the electrostatic components are all repulsive, they show a direct correlation with inhibitor activity as measured by $\Delta G_{\text{binding}}$. The role of γ is primarily to produce an overall negative binding energy, and it can effectively be replaced with a negative constant. During the MC simulations of the unbound solvated inhibitors, the R^6 and S^6 absolute conformations do not interconvert due to the formation of a favorable hydrogen bond to solvent. In the complex, however, interconversion of these conformations of the inhibitor is observed during the course of the simulations, a phenomenon which is apparently not observed in the crystalline state of the complex. Hydrogen bonding of the inhibitor to the backbone NH of K101 and the lack of such an interaction with the C═O of K101 or with solvent correlate with enhanced activity, as does the ability to assume a number of different orientations of the inhibitor dimethylallyl moiety with respect to residues Y181 and Y188 while retaining contact with W229. Overall, the use of a combination of MC simulation with a linear response method shows promise as a relatively rapid means of estimating inhibitor activities. This approach should be useful in the preliminary evaluation of potential modifications to known inhibitors to enhance activity.

Introduction

The reverse transcriptase (RT) of HIV-1 has been an active target for drug development for a number of years. Two major classes of inhibitors have been reported: nucleoside inhibitors (NIRT) such as zidovudine (AZT) and nonnucleoside inhibitors (NNIRT) such as the derivatives of tetrahydroimidazo[4,5,1-*jk*][1,4]benzodiazepine-2(1*H*)-thione and -one (TIBO; Table 1, **1g** and **1l**). Both the mode of action and the binding site are different for these two classes of inhibitors. Nucleoside analogues are competitive inhibitors that irreversibly terminate extension of the primer strand of the polymerase reaction and bind in the polymerase active site.[1] Nonnucleoside inhibitors are, for the most part, noncompetitive inhibitors[2] and bind noncovalently in a site different from, but proximal to (∼15 Å), the site of the polymerase reaction. Inhibitors in the latter class are particularly attractive drug candidates in that their binding site is unique to the reverse transcriptase of HIV-1, and thus they are less likely to cause adverse side effects by disruption of normal DNA polymerase activity.

A number of crystal structures exist for various forms of RT: alone,[3] in combination with DNA,[4] and in combination with a variety of NNIRT inhibitors,[5] including two (**1a** and **1f**) derivatives of TIBO.[5d,f] From those data it can be seen that RT is a relatively flexible protein. The NNIRT binding pocket does not exist as such in structures that do not contain an NNIRT.[5d] Complexation with inhibitors of this class results in the creation of a common binding pocket, bound on virtually all sides by protein residues. Only a narrow channel, suggesting the point of initial inhibitor entry, permits contact of the bound inhibitor with solvent.

Most known NNIRT inhibitors share a common "butterfly" shape[5d] consisting of two (or more) "wings",

‡ Western Maryland College.
† NCI−Frederick Research and Development Center.
§ Yale University.
▽ Janssen Research Foundation.

10.1021/jm9804174 CCC: $15.00 © 1998 American Chemical Society
Published on Web 12/01/1998

Table 1. Structure and IC_{50} Values for TIBO Inhibitors of HIV-1 RT

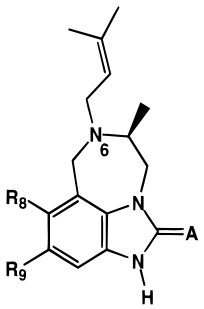

compd	R_8	R_9	A	IC_{50} (mM)
1a	Cl	H	S	0.0043
1b	F	H	S	0.0058
1c	methyl	H	S	0.0136
1d	ethynyl	H	S	0.0295
1e	methoxy	H	S	0.0339
1f	H	Cl	S	0.0340
1g	H	H	S	0.0440
1h	CN	H	S	0.0563
1i	ethynyl	H	O	0.4371
1j	methyl	H	O	0.9890
1k	CN	H	O	1.1400
1l	H	H	O	3.1550

more specifically π-electron-containing moieties, that do not share a common plane. In general these π-systems are aromatic rings; however, in TIBO derivatives one wing is simply a dimethylallyl moiety. Within the common binding site, existing crystal structures and molecular modeling studies show that the amino acid residues adopt somewhat different orientations for inhibitors of even very similar structure.[5d−f,6] Consequently the term "shrink-wrap" has been used to describe the unique accommodation of the protein to different inhibitors.[6]

Binding of an NNIRT inhibitor to the enzyme is believed to result in an alteration of the optimum geometry of the substrates (nucleic acid template-primer and nucleoside triphosphate) and protein residues (including two Mg^{2+} ions) at the site of the polymerase reaction.[4,5a] Crystallographic evidence shows a substantial difference in the conformation of the NNIRT−RT complex from that of either RT alone or complexed with a strand of duplex DNA.[4,5d,e] This allosteric effect of the inhibitor may lower the efficiency of formation of the requisite sugar−phosphate bond that is central to the polymerase reaction. Other effects, such as alteration of the K_d for the enzyme−substrate binary and ternary complexes, could also be operative. Nonetheless, it is reasonable to assume that an effective NNIRT inhibitor will be one that binds strongly to the enzyme and, upon binding, results in deleterious alteration of the geometry at the polymerase site. While the kinetics of NNIRT inhibition of RT are complex,[7] it appears that knowledge of the strength with which the inhibitor binds to the enzyme is germane.

The development of efficient computational methods for the estimation of free energies of binding for enzyme−inhibitor complexes has been an area of active investigation in the search for new and more effective inhibitors. Energy minimization approaches to the current problem offer the advantage of being relatively rapid and have yielded valuable information.[6,8] These methods, however, generally rely upon single structures for the unbound inhibitor and the complex and thus suffer from the difficulty of locating an appropriate local minimum for these species. Of necessity, a single structure is incapable of representing the range of ligand and protein flexibility found in solution.

In recent years a number of methods have relied upon free energies calculated from averages based on thermally equilibrated collections of configurations. These populations are generated either deterministically through molecular dynamics (MD) or stocastically by Monte Carlo (MC) simulations. Using ensembles thus obtained, reasonably accurate absolute binding free energies have been estimated from a linear response (LR) assumption for a combination of electrostatic and van der Waals nonbonded interaction terms.[9] In some cases a cavitation penalty term has also been included in the relationship.[10]

Essentially, MD−LR and MC−LR methods evaluate the nonbonded interaction energy of the inhibitor with its environment. In the case of the unbound inhibitor, this environment consists solely of the solvent. For the bound inhibitor, the environment includes not only solvent but also the surrounding protein. Thus a typical LR equation takes the form:

$$\Delta G_{\text{binding}} = \alpha(\langle U^{\text{vdw}}_{\text{bound}}\rangle - \langle U^{\text{vdw}}_{\text{unbound}}\rangle) + \beta(\langle U^{\text{elec}}_{\text{bound}}\rangle - \langle U^{\text{elec}}_{\text{unbound}}\rangle) \quad (1)$$

The terms $\langle U^{\text{vdw}}\rangle$ and $\langle U^{\text{elec}}\rangle$ refer to the Lennard−Jones and electrostatic average interaction energies for the bound and unbound states of the inhibitor. The coefficients α and β are either assigned or empirically determined to obtain the best fit to the experimental observable, the free energy of binding. While a theoretical case can be made for a value of 0.5 for β, it has been argued that this value can vary depending upon the structural/polar nature of the inhibitor[11] and the particular force field employed.[12] In some cases a third term is included to account for the cost of creating a cavity in the environment. This has been necessary particularly in cases such as alkanes where ΔG_{hyd} is positive.[10,13]

$$\Delta G_{\text{binding}} = \alpha(\langle U^{\text{vdw}}_{\text{bound}}\rangle - \langle U^{\text{vdw}}_{\text{unbound}}\rangle) + \beta(\langle U^{\text{elec}}_{\text{bound}}\rangle - \langle U^{\text{elec}}_{\text{unbound}}\rangle) + \gamma(\langle \text{SASA}_{\text{bound}}\rangle - \langle \text{SASA}_{\text{unbound}}\rangle) \quad (2)$$

Based upon the change in solvent-accessible surface area (ΔSASA) of the inhibitor during complexation, this term is $\gamma\langle\Delta\text{SASA}\rangle$, with γ being a third coefficient to be fit empirically to the experimental data.

The present study involves the application of the above LR approach to MC-generated assemblies of configurations of the species involved in the complexation of one class of NNIRT inhibitors, derivatives of TIBO, with HIV-1 reverse transcriptase. A total of 12 substituted TIBO derivatives, shown in Table 1, have been included in this study. The goal is to determine if binding energies estimated in this fashion can be correlated with experimental IC_{50} values, a measure of the ability of the inhibitor to retard the polymerase action of the enzyme.

Computational Method

Inhibitor Structure. A number of different conformations can be considered for the basic TIBO structure. The *S* absolute configuration at C5 is crucial for activity against HIV-1 RT. A

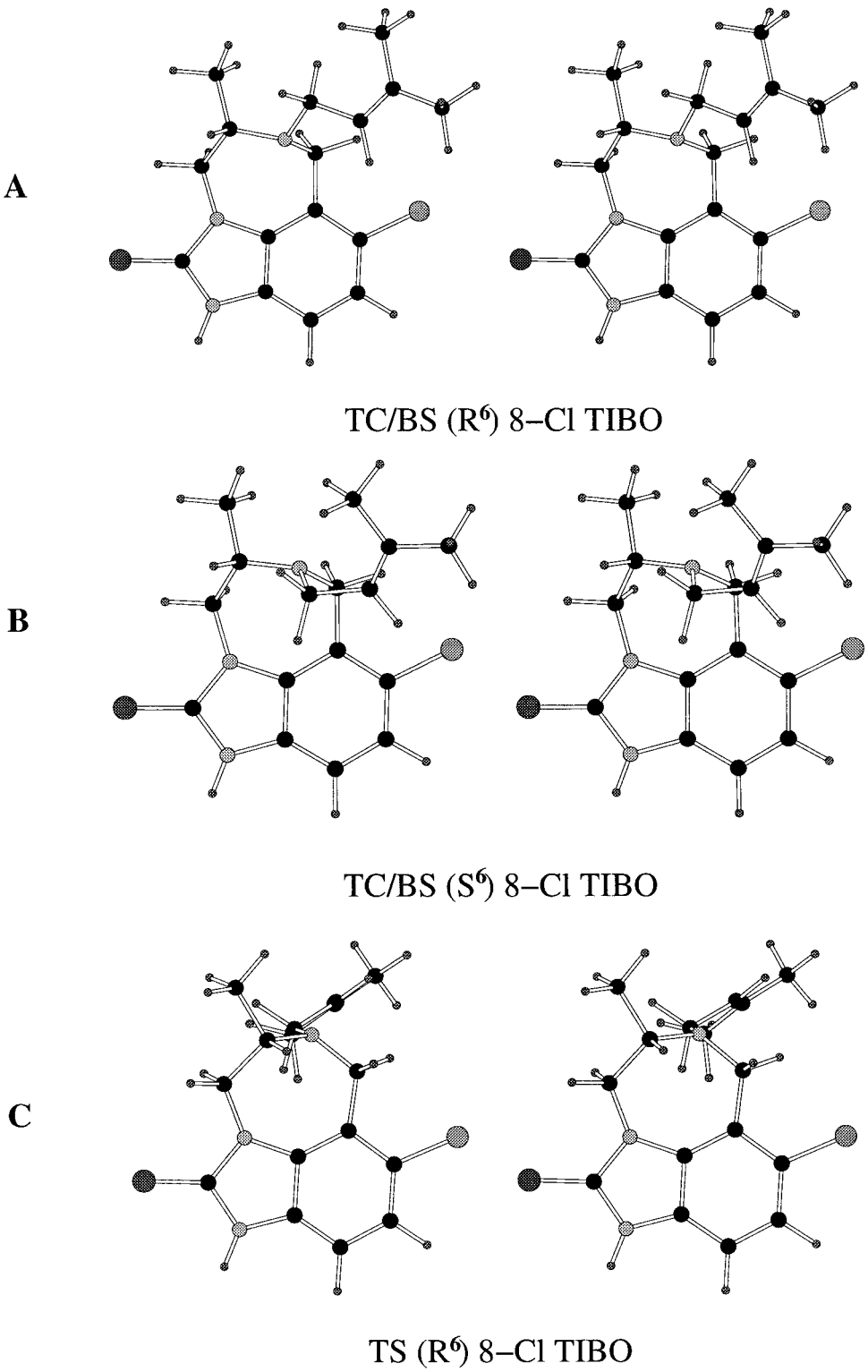

Figure 1. Stereoplots of AM1-minimized (S^5)-8-Cl TIBO conformations. R^6 and S^6 refer to the absolute conformation of N6.

crystal structure of S^5-9-Cl TIBO has been published[14] which shows the presence of two different conformations of the diazepine ring. In one, the TS conformation[14,15] (Figure 1C), C5 and N6 lie on opposite sides of the plane of the ring, reminiscent of the twist conformation of cyclohexane. In the second conformation (Figure 1A), TC/BS,[14,15] C5 and N6 both lie on the same side of the plane, somewhat analogous to the boat conformation of cyclohexane. In both of these conformations, N6, which is presumably capable of inversion, was reported only as existing in the *R* absolute conformation in the crystal. NMR studies (methanol-d_6) from this same report indicate a 90:10 mixture of two species in solution. On the basis of semiempirical PM3 calculations, the authors[14] determined the TS conformation to be more stable and thus assigned that

structure to the more populated species in methanol solution. In confirmation of this trend, we have found the (S^5,R^6)-TS conformation (−1637.8743853 Hartrees) of 8-Cl TIBO to be 0.82 kcal/mol more stable than the (S^5,R^6)-TC/BS conformation (−1637.8730791 Hartrees) at the 6-31G* ab initio level of theory.

Considering the structures A and C in Figure 1, however, it can be seen that the TS (C) and TC/BS (A) conformations differ significantly in the orientation of the dimethylallyl side chain. Interconversion would require extensive molecular motion to shift this moiety from one side of the ring plane to the other. In the 8-Cl and 9-Cl TIBO complexes with RT,[5d,f] the structure of the inhibitor is (S^5,R^6)-TC/BS (A). It seems reasonable to assume that the conformation of the inhibitor that enters the protein would be similar to that found in the RT complex. Once within the protein, molecular motions of the inhibitor would be significantly restricted and TS-to-TC/BS conversion would appear unlikely. Thus the TC/BS conformation was chosen as the initial structure for the unbound inhibitor calculations. It should be noted that, in the (R^6)-TC/BS conformation, the nitrogen lone pair lies over the diazepine ring and is directed toward the aromatic rings, while in the (R^6)-TS conformation it is directed away from the tricyclic ring system. (The designation of this absolute conformation of N6 is based upon assigning the lone pair the lowest priority in the Kahn−Ingold−Prelog system. The authors of the crystallographic study[14] assigned these structures as *S*, apparently following a different convention.)

In Figure 1, it can be seen that a second TC/BS structure (B) of almost identical overall shape to conformation A can be obtained in which N6 has the *S* absolute conformation (Figure 1B). In this structure, (S^6)-TC/BS, the N6 nonbonded pair is directed away from the aromatic rings. Only minor bond rotations are required to invert N6 and interconvert these two diastereomers. Gas-phase ab initio geometry optimizations (using the Gaussian94 program[16]) for these similarly shaped R^6 and S^6 conformations of **1a**−**1l** show the R^6 structure consistently to be the more stable (data included in Supporting Information). Across the series, the difference ranges from significant (1.4 kcal/mol, **1h**) to negligible (0.01 kcal/mol, **1l**). Consequently, it seemed prudent to include consideration of both the R^6 and S^6 structures for the unbound inhibitor.

Two pK_a values have been determined experimentally for 8-Cl TIBO[17] (**1a**): pK_{a1} = 9.5, pK_{a2} = 6.3. Thus the majority of the unbound inhibitor will exist in the monoprotonated state in solution at physiological pH. The most probable site for protonation is N6, the tertiary amino nitrogen. It is unlikely, given the hydrophobic nature of the RT binding pocket, that the bound inhibitor is protonated; thus the conjugate acid of the inhibitor must lose a proton before entering the protein. An acidic residue, E138 of p51, is situated at the putative site of entry and thus may function in this capacity. To test the possible role of the protonated form of the inhibitor, the unbound conjugate acids of TIBO were also investigated.

Monte Carlo Simulations. For each inhibitor, two MC simulations were performed, one for the unbound inhibitor in solvent and a second with the inhibitor bound in a model of the NNIRT binding pocket of RT in solvent. All calculations were performed using the program MCPRO[18] implemented on R10000 Silicon Graphics workstations.

1. Unbound Inhibitors. The starting conformation for the unbound inhibitor simulations was obtained by gas-phase AM1 minimization of the (R^6)-TC/BS conformation of 8-Cl TIBO, as it is found in its crystallographic complex with HIV-1 reverse transcriptase.[5d,f] Subsequent 6-31G* minimization produced only a 0.04-Å rms heavy atom change in those portions (see later) of the molecule that were held fixed in the MC simulations. The AM1 (as opposed to 6-31G*)-minimized structure was chosen as the starting structure because it contained the dimethylallyl side chain in an orientation that was slightly closer to that in the crystal structure of the RT/8-Cl TIBO complex. Test calculations revealed no significant difference in the resultant energies regardless of which minimized structure was used as the starting conformation for the inhibitor. The S^6 conformation was obtained by manual alteration of the appropriate bond angles to generate the structure B shown in Figure 1, followed by AM1 minimization. Structures for the N6-protonated conjugate acid of the R^6 and S^6 conformations were obtained simply by addition of the requisite proton in the same orientation as the lone pair in the respective neutral compounds. Appropriate atom substitutions were then made to these four basic structures to modify the group on position 8 (or 9) of the benzene ring. Thus four series of inhibitors were generated: neutral R^6, neutral S^6, and their conjugate acid analogues.

All atoms of the inhibitor were explicitly included. The majority of the parameters for the inhibitor were assigned from the OPLS all-atom force field.[19] The exceptions were for the dihedral torsion parameters for the CNCC and CN^+CC dihedral angles. These were determined by fitting the MM3-generated dihedral profile for 15° incremental rotation about the CNCC bond of *N*,*N*′-dimethylethanamine and the *N*,*N*′-dimethylethanammonium ion. Energy minimization was carried out at each step in the rotation. Appropriate parameters were then obtained to match these profiles to analogous OPLS all-atom force-field-minimized profiles from the BOSS program[20] lacking the CNCC dihedral term: V_0, V_1, V_2, V_3 (kcal/mol) = 0.0, −2.389, 1.753, 0.982 (CNCC); 0.0, 1.109, 0.127, 0.212 (CN^+CC).

In all of the linear response models discussed above, much emphasis is placed upon the electrostatic nonbonded interaction term, U^{elec}. Thus the determination of partial charges on the atoms of the inhibitor is critical. Carlson and Jorgensen[10] found good correlation for ΔG_{solv} using electrostatic potential surface (EPS) charges from 6-31G* ab initio calculations, and this method was used in the present study to determine partial charges. In calculations of this type, however, care must be exercised to select a molecular conformation that is relevant to the system for which the charges are intended. Thus, partial charges for each R^6 and S^6 neutral inhibitor and its conjugate acid were obtained using the ChelpG routine[21] in the Gaussian94 program by fitting to the EPS from ab initio full geometry optimizations with the 6-31G* basis set.

The thiazolobenzimidazole ring system and the six atoms associated with the allylic double bond were held internally rigid during the MC simulations owing to the assumption that variations in the geometry of these portions of the inhibitor would be minimal. Because these regions were linked by geometry elements that vary, they could, however, move relative to one another and would of course follow rigid body motions of the inhibitor. For the aqueous simulations, the inhibitor was surrounded by a 26-Å sphere of 2434 TIP3P waters. A 1.5 kcal/mol harmonic restraining force was applied to waters at the surface of the sphere to prevent their escape.

MC simulations of the unbound inhibitors consisted of an initial solvent equilibration of 10×10^6 configurations in which the solute remained fixed, followed by an additional 10×10^6 configurations of equilibration in which the inhibitor was also permitted to move. Energy averages were then accumulated over a final 10×10^6 configurations, during which atomic coordinates were saved after each 2×10^5 configurations. Separate running averages were maintained for the Lennard−Jones and Coulombic components of the solute−solvent nonbonded interaction energies throughout the simulation. The standard deviation for each of these components during the energy-averaging phase was ≤1.5% of the mean, indicating that the system had apparently equilibrated. As has been previously observed, electrostatic interaction energies showed slightly greater variation than did van der Waals energies. The average SASA[22] and absolute conformation of N6 were determined for the geometry snapshots from the final energy-averaging phase of the simulation. In determining the SASA, the atomic radii for the all-atom representation of the inhibitor were calculated based on OPLS all-atom σ nonbonded parameters using radius = $2^{1/6} \times \sigma/2$ and a solvent radius of 1.4 Å, as implemented in MCPRO.

2. RT−Inhibitor Complexes. The model for the complex of inhibitor and RT was based on the crystal structure of 8-Cl

Table 2. Average Interaction Energies from Bound and Unbound Neutral Inhibitor MC Simulations (kcal/mol)

	U^{elec}				U^{vdW}			
inhibitor	$inhib_{bd}$−solv	$inhib_{bd}$−enz	R^6 $inhib_{unbd}$−solv	S^6 $inhib_{unbd}$−solv	$inhib_{bd}$−solv	$inhib_{bd}$−enz	R^6 $inhib_{unbd}$−solv	S^6 $inhib_{unbd}$−solv
1a	4.06	−23.13	−22.14	−22.06	−1.60	−47.22	−30.58	−29.31
1b	4.74	−24.19	−26.86	−26.60	−1.66	−44.55	−29.19	−29.47
1c	3.79	−20.53	−26.04	−22.04	−1.98	−49.59	−29.62	−31.27
1d	1.82	−23.73	−30.67	−26.04	−1.64	−51.02	−31.18	−30.38
1e	6.78	−25.17	−29.52	−28.88	−2.11	−47.73	−31.66	−30.53
1f	6.88	−20.93	−27.66	−25.62	−2.17	−46.51	−30.76	−30.89
1g	3.24	−25.09	−22.61	−26.50	−2.45	−45.89	−29.73	−28.43
1h	2.82	−21.79	−32.16	−37.81	−0.95	−50.21	−28.77	−29.00
1i	4.34	−21.93	−28.91	−36.72	−2.09	−49.15	−29.65	−27.69
1j	4.26	−20.49	−32.04	−28.35	−2.66	−47.67	−28.07	−29.60
1k	4.15	−20.86	−35.35	−34.52	−1.79	−49.62	−28.34	−26.63
1l	4.28	−19.45	−26.14	−29.96	−1.88	−45.86	−27.13	−26.69
SD[a]	0.29	0.17	0.47	0.51	0.06	0.18	0.23	0.24

[a] Average standard deviation from batch means calculations for all inhibitors.

TIBO/HIV-1 reverse transcriptase.[5d] From this structure and in a fashion previously reported,[6] a model of the inhibitor binding pocket was constructed from amino acid residues roughly within 20 Å of the inhibitor. This resulted in 133 amino acid residues in eight strands, terminated with either an acetyl or methylamino group at their N- and C-terminal ends, respectively. Basic (Arg and Lys) and acidic (Asp and Glu) residues were assumed to be in their charged states. These criteria led to the inclusion of amino acid residues mainly from the p66 domain of RT, with one short segment from the p51 domain. All amino acid residues within 10 Å of the inhibitor were permitted to vary, while more distant residues remained fixed during minimization and MC simulations. The amino acid residues comprising the site were thus: (flexible) from the p66 domain 94−111, 176−193, 223−237, and from p51 136−138; (fixed) from p66 90−93, 112−113, 157−175, 194−206, 214−222, 238−242, 266−270, 314−322, 347−350, 381−383, and from p51 133−135, 139−141. This structure was initially minimized using the AMBER force field in the Discover module of InsightII (Molecular Simulations, Inc.). The three-stage minimization protocol for this calculation was the same as that previously reported.[6] The geometry of 8-Cl TIBO in this structure was then replaced by that of the AM1-minimized unbound R^6 conformation of the inhibitor. These structures differed only very slightly in geometry, but this replacement was deemed prudent in order that the internal geometry of fixed portions of the inhibitor would be the same in both bound and unbound simulations.

For MC simulations, the protein−ligand complex was partially surrounded in a 26-Å sphere of 1592 TIP3P water molecules that was centered at the geometric center of the inhibitor. This resulted in the inhibitor and all variable amino acid residues being surrounded by at least 10 Å of water and/or fixed amino acid residues. A 9-Å cutoff distance was used for all nonbonded interactions. For the protein, a partial united atom approach[12,23] was used in which all hydrogens are explicit except those on saturated carbon atoms. The backbone conformation and all bond lengths of the protein were fixed throughout the MC simulations. In a fashion similar to the unbound inhibitor calculations, the above-derived conformation and orientation (in the binding pocket) of the 8-Cl TIBO/RT complex was used as the template for structural modification to the variously substituted TIBO derivatives. None of the structural modifications to the inhibitor led to van der Waals overlap with the protein, and thus no subsequent positional adjustments were required.

Simulations for the bound inhibitor−protein complex consisted of three phases: 10×10^6 configurations of equilibration with only water moving, 4×10^6 configurations of equilibration in which the inhibitor and protein (partially constrained as described above) were also allowed to move, and a final 8×10^6 configurations during which energy averages and geometry snapshots were acquired. Separate running averages were obtained for the Lennard−Jones and Coulombic components for both inhibitor−solvent and inhibitor−protein nonbonded interactions. As in the case of the unbound inhibitor simulations, the standard deviations for each of these components was ≤1.5% of the mean. The average SASA, individual absolute conformation of N6, H-bond distances, and orientation of the dimethylallyl moiety were determined from these snapshots.

Inhibitor Activity. The IC_{50} values for most of the inhibitors in Table 1 have been reported previously.[24] Additional data were kindly provided by the authors of that study. These values were then converted to estimated experimental free energy values using the standard $\Delta G_{binding} = -RT \ln K_{form}$ relationship at 37 °C. Here K_{form}, the equilibrium constant for the formation of the complex, is taken to be the reciprocal of the IC_{50} value. This estimate was required because K_i data are not available for TIBO complexes with RT. Given the very close similarity in structure and presumed mechanism of action of the inhibitors in this study, however, it is reasonable to expect that IC_{50} and K_i, while not equivalent, should be linearly related[25] for this series of TIBO derivatives.

Results and Discussion

Inhibitor Conformation. Throughout the MC simulations of all of the unbound inhibitors, it was found that the diazepine ring system remained in the TC/BS conformation. Further, it was observed that N6 did not invert from its initial R^6 conformation. In part, this could be due to unfavorable energy terms associated with the N6 planar transition state, a requisite for R^6 to S^6 conversion. Gas-phase 6-31G* ab initio calculations, however, showed that the planar N6 conformation of the TC/BS conformation of **1g** lies 1.75 kcal/mol above the R^6 conformer and 1.50 kcal/mol higher than the S^6 form. Given this surprisingly low barrier, the explanation for the lack of inversion during MC simulations likely lies in the observation that in approximately one-half of the acquired geometry snapshots there exists a H-bond between N6 and a solvent water molecule. Traversing the N6 planar transition state barrier would involve a diminution of this favorable energy term, thus increasing the effective barrier to N6 inversion.

In contrast, N6 inversion does occur in many of the simulations of the inhibitor−protein complexes. Analysis of the conformation of N6 in the geometry snapshots showed that in those cases where R to S inversion is observed, the inhibitor passes over this barrier in both directions a number of times during the simulation. The data in Table 3 show that the extent to which one absolute conformation is sampled versus the other varies throughout the series, with no obvious structure-based pattern to these variations. It is interesting to

Table 3. Percentage Bound (R^6)-TIBO Configuration[a] and Calculated Average SASA (Å^2) for Bound and Unbound Neutral Inhibitors

compd	% R^6_{bd}	$SASA_{bd}$	R^6 $SASA_{unbd}$	S^6 $SASA_{unbd}$
1a	8	44.4	558.0	561.3
1b	5	43.4	551.4	552.7
1c	30	40.6	554.7	548.6
1d	82	57.2	565.3	597.6
1e	100	62.4	591.8	576.5
1f	48	37.2	579.8	558.8
1g	2	21.2	550.8	541.4
1h	40	40.6	579.0	569.8
1i	85	74.3	567.5	553.0
1j	62	22.4	540.8	542.5
1k	100	24.1	540.8	534.5
1l	72	32.4	531.2	537.6
SD[b]		28.1	7.5	9.5

[a] Unbound inhibitor shows no inversion of N6. [b] Average standard deviation for all inhibitors.

note that this interconversion appears to be retarded in crystals of the complex in that only the R^6 conformation is seen.[5d,f] As in the unbound simulations, the diazepine ring system remained in the TC/BS conformation in the complex.

Linear Response Investigation. From the MC simulations, average electrostatic and van der Waals interaction energies were determined between the unbound R^6 and S^6 inhibitors and R^6 bound inhibitors **1a**−**1l** and their surrounding environments (see Table 2). The average SASA was also determined for the saved representative structures (Table 3). The data in Tables 2 and 3 were then used to evaluate the fit to experimental $\Delta G_{binding}$ values with various forms of the LR eqs 1 and 2. It will be recalled that α, β, and γ are weighting parameters for the van der Waals, electrostatic, and SASA terms, respectively.

The results based on the R^6 unbound inhibitor will be considered first. Using eq 1 or 2 with previously reported[9a,b,10,12] values of α, β, and γ gave poor prediction of experimental $\Delta G_{binding}$, with root-mean-square (rms) errors between experimental and calculated $\Delta G_{binding}$ ranging between 12.13 and 2.03 kcal/mol. Given a total range in experimental $\Delta G_{binding}$ of only 4.06 kcal/mol, it was clear that reparametrization was needed to improve the estimates.

Determination of new α, β, and γ parameters for the various LR equations was accomplished by a least-squares fitting routine. The results of the various models for fitting the MC simulation data to the experimental binding energies are shown in Table 4. Reparameterizing eq 1 for both α and β (model 1) gave a slight improvement (rms error 1.71).

Reparametrization of eq 2 for all coefficients (model 2) gave a significantly improved fit (rms error 0.87). A plot of these results and the associated least-squares line is shown in Figure 2. The coefficient α, however, was negative (−0.139), a value which seems unreasonable on physical grounds. Setting $\alpha = 0$ and reparameterizing for β and γ (model 3) also produced a very good estimate of binding energies, rms error 0.91. It might be argued, however, that this approach is also counterintuitive in that it ignores the Lennard−Jones contribution to binding. Arbitrary assignment (model 4) of a small but significant weight to the Lennard−Jones component, $\alpha = 0.100$, and reparametrization of β and γ did not dramatically degrade the fit (rms error 0.98).

The difficulty in achieving reasonable values for α and β is perhaps best seen by comparison of the unweighted changes in the van der Waals (α) and electrostatic (β) interactions energies for the complexation reaction (Table 5). The van der Waals terms are all highly attractive but do not follow any clear pattern across the series of inhibitors. If anything, the less active inhibitors have more favorable van der Waals interactions. Hence, any inclusion of this term in the model worsens the accuracy of the estimate. On the other hand, while the electrostatic components are all repulsive, the value of this term correlates in a rational fashion with inhibitor activity. Thus, while electrostatic interactions roughly predict the correct orderings of inhibitor activities, to compensate for their repulsive character, there appears to be a relatively large negative component missing from the model. Inclusion of the cavitation term supplies that component.

An alternative approach is to supply this negative component in a model that replaces the ΔSASA term with a constant, δ.

$$\Delta G_{binding} = \alpha(\langle U^{vdw}_{bound}\rangle - \langle U^{vdw}_{unbound}\rangle) + \beta(\langle U^{elec}_{bound}\rangle - \langle U^{elec}_{unbound}\rangle) + \delta \quad (3)$$

The results of this approach are very similar to, but slightly less predictive than, the analogous models based on eq 2. Fitting both α and β (model 2a) again produces a presumably unreasonable negative value for α (rms error 0.93). Neglecting α (model 3a) gives a slightly poorer fit (rms error 1.00), and assigning α the value of 0.100 (model 4a) is even less predictive (rms error 1.07).

Overall, assuming all parameters should be positive, the best model (3) is one that includes only the electrostatic and SASA components, $\beta = 0.171$ and $\gamma = 0.0229$, rms error 0.91. If one assumes for the sake of potential applicability to other systems that a positively weighted Lennard−Jones term should be present in the final relationship, then models 4 and 4a are reasonable candidates. The value for β in these two models is similar, the average being 0.192. Of the two, model 4 is slightly better at estimating $\Delta G_{binding}$ for the present system, rms error 0.98.

Results of a LR analysis of the data in which values for the R^6 unbound inhibitors are replaced with those for the S^6 unbound inhibitor lead to essentially the same conclusions (Table 6). Poor fits again are obtained with previously published parameters. In all of the models that incorporate a SASA term, the S^6 unbound MC simulation data produce a slightly higher rms error than do those for the R^6 unbound inhibitor. The opposite is true for models that substitute a constant, δ, for the SASA term. Consideration of the unweighted components (Table 5) again reveals highly attractive van der Waals components that run counter to the order of inhibitor activity and replusive electrostatic values that correlate directly with observed binding energies. The values for β are slightly smaller than those obtained with the R^6 unbound inhibitor data, e.g., for model 3, $\beta = 0.133$ (S^6) compared with 0.171 (R^6). It is reassuring, however, that the accuracy of the prediction and the estimated values of the parameters are similar, irrespective of whether the LR is based on the unbound R^6 or S^6 inhibitor simulations. This suggests a rather

Table 4. Comparison of Experimental and Calculated $\Delta G_{binding}$ for Various Parameter-Fitting Models Using R^6 Neutral Unbound Inhibitors

model	1	2	3	4	2a	3a	4a	
eq	1	2	2	2	3	3	3	
α	0.624	−0.139	0.000	0.100 const	−0.225	0.000	0.100 const	
β	0.261	0.136	0.171	0.196	0.108	0.164	0.189	exptl
γ	0.000	0.0276	0.0229	0.0195	0.000	0.000	0.000	
δ					−15.769	−11.783	−10.013	
1a	−10.59	−11.25	−11.25	−11.25	−11.33	−11.28	−11.26	−11.87
1b	−8.69	−10.67	−10.38	−10.16	−11.14	−10.57	−10.32	−11.69
1c	−11.28	−9.90	−10.19	−10.40	−9.82	−10.26	−10.46	−11.16
1d	−11.12	−9.87	−10.14	−10.34	−9.99	−10.35	−10.51	−10.69
1e	−8.44	−10.60	−10.23	−9.96	−10.48	−9.96	−9.73	−10.60
1f	−7.64	−10.66	−10.11	−9.71	−10.27	−9.56	−9.24	−10.60
1g	−11.41	−11.96	−12.01	−12.04	−11.50	−11.66	−11.73	−10.44
1h	−10.54	−9.99	−10.09	−10.16	−9.31	−9.63	−9.77	−10.29
1i	−10.52	−9.10	−9.37	−9.56	−9.69	−9.93	−10.04	−9.02
1j	−9.77	−9.09	−9.18	−9.24	−9.06	−9.20	−9.26	−8.52
1k	−9.54	−8.55	−8.66	−8.73	−8.57	−8.73	−8.81	−8.43
1l	−10.00	−9.44	−9.56	−9.64	−9.95	−9.99	−10.01	−7.81
rms error	1.71	0.87	0.91	0.98	0.93	1.00	1.07	

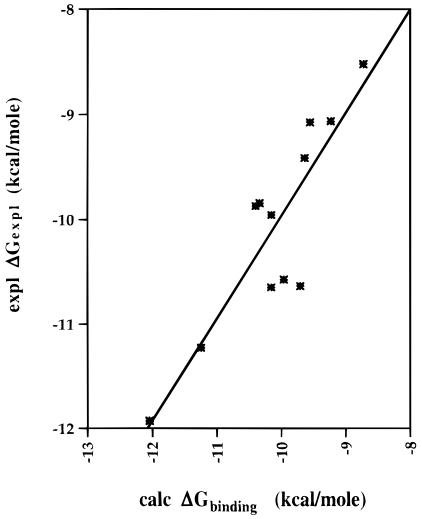

Figure 2. Plot of calculated and experimental $\Delta G_{binding}$ for R^6 neutral inhibitor complexation (Table 4, model 2).

Table 5. Unweighted Changes in Energy and SASA from MC Simulations[a] Using Bound and Unbound Neutral Inhibitors

	R^6 inhibitor			S^6 inhibitor		
compd	ΔU^{elec}	ΔU^{vdW}	ΔSASA	ΔU^{elec}	ΔU^{vdW}	ΔSASA
1a	3.06	−18.24	−513.6	2.98	−19.52	−516.9
1b	7.42	−17.02	−508.0	7.15	−16.74	−509.3
1c	9.30	−21.96	−514.0	5.30	−20.30	−508.0
1d	8.77	−21.48	−508.0	4.14	−22.28	−540.4
1e	11.13	−18.18	−529.5	10.49	−19.31	−514.1
1f	13.61	−17.93	−542.6	11.57	−17.80	−521.6
1g	0.77	−18.60	−529.6	4.65	−19.91	−520.2
1h	13.18	−22.40	−538.4	18.83	−22.16	−529.2
1i	11.32	−21.59	−493.2	19.12	−23.55	−478.7
1j	15.81	−22.25	−518.4	12.12	−20.72	−520.1
1k	18.64	−23.07	−516.7	17.80	−24.78	−510.4
1l	10.96	−20.60	−498.8	14.78	−21.04	−505.2

[a] R^6 and S^6 sections of the table refer to calculations based on the respective inhibitor simulations.

robust LR relationship that is capable of predicting binding energies with a rms error of 0.9 and 1.0 kcal/mol.

Inhibitor Protonation State. Structurally, TIBO derivatives are tertiary amines that also bear a benzimidazole moiety. As such, there are three potential sites for protonation in the near-neutral pH range, the benzylic nitrogen (N6) and the tertiary nitrogens (N1 and N3) of the imidazole ring. As was previously noted, two pK_a values have been determined for 8-Cl TIBO[17] (**1a**): pK_{a1} = 9.5, pK_{a2} = 6.3. Given a pK_a for benzylamine[26] of 9.34, it is reasonable to assume that pK_{a1} is the acidity constant for the singly charged conjugate acid bearing a proton on N6 and pK_{a2} is the corresponding value for the diprotonated species bearing an additional proton on the imidazole ring. At pH 7.5, the dominant species present in solution would be the N6-monoprotonated species. It is not known whether the neutral or protonated form of the inhibitor reacts with the enzyme in the complexation reaction. For all but the 8-MeO, **1b**, and 9-Cl, **1e**, protonated inhibitors, the gas-phase 6-31G* RHF energies (data in Supporting Information) show the R^6 conformation to be more stable than the S^6 form, with the largest difference being 1.43 kcal/mol. It seemed reasonable, therefore, to explore the existence of a LR relationship based upon solvation energies of the N6-protonated form of the unbound inhibitor in both the R^6 and S^6 conformations.

The electrostatic and van der Waals components and SASA values from the MC simulations for 10 of the 12 inhibitors are listed in Tables 7 and 8, respectively. The ethynyl derivatives **1d** and **1i** were not included in this study. Unweighted changes in these terms for the complexation reaction are presented in Table 9. In these calculations, the inhibitor in the complex was assumed to be neutral. The ΔU^{vdw} values are attractive and similar in magnitude to those for the neutral inhibitors (Table 5) and again show no clear pattern across the series of inhibitors. As might be expected given the favorable solvation of a cationic species, the ΔU^{elec} values are now significantly more repulsive than in the neutral case. There still remains, however, a general trend that more active inhibitors have lower ΔU^{elec} values. Data are shown in Tables 10 and 11 for the reparametrization attempts using the same models as those in the neutral unbound inhibitor series. In each case the fit is poorer than that obtained from either of the neutral conformations (Tables 4 and 6) of the inhibitors. This difference is not sufficient, however, to shed light on the possible involvement of the protonated species in the complexation reaction.

Because the charge on the unbound (+1) and bound

Table 6. Comparison of Experimental and Calculated $\Delta G_{binding}$ for Various Parameter-Fitting Models Using S^6 Neutral Unbound Inhibitors

model	1	2	3	4	2a	3a	4a	
eq	1	2	2	2	3	3	3	
α	0.607	−0.162	0.000	0.100 const	−0.187	0.000	0.100 const	
β	0.243	0.092	0.133	0.159	0.118	0.159	0.180	
γ	0.000	0.0280	0.0224	0.0189	0.000	0.000	0.000	
δ					−15.232	−11.799	−9.964	exptl
1a	−11.13	−11.06	−11.18	−11.25	−11.23	−11.33	−11.38	−11.87
1b	−8.43	−10.91	−10.45	−10.17	−11.25	−10.66	−10.35	−11.69
1c	−11.05	−10.46	−10.67	−10.79	−10.81	−10.96	−11.04	−11.16
1d	−12.53	−11.16	−11.55	−11.79	−10.58	−11.14	−11.45	−10.69
1e	−9.18	−10.32	−10.11	−9.98	−10.38	−10.13	−10.00	−10.60
1f	−8.00	−10.67	−10.14	−9.80	−10.53	−9.96	−9.66	−10.60
1g	−10.96	−10.93	−11.03	−11.09	−10.96	−11.06	−11.12	−10.44
1h	−8.89	−9.51	−9.34	−9.23	−8.86	−8.81	−8.78	−10.29
1i	−9.66	−7.85	−8.17	−8.37	−8.56	−8.76	−8.87	−9.02
1j	−9.65	−10.11	−10.03	−9.98	−9.92	−9.87	−9.85	−8.52
1k	−10.73	−8.66	−9.05	−9.30	−8.49	−8.97	−9.23	−8.43
1l	−9.19	−9.39	−9.34	−9.31	−9.55	−9.45	−9.40	−7.81
rms error	1.69	0.88	0.93	1.01	0.83	0.90	0.98	

Table 7. Average Interaction Energy and SASA from MC Simulations[a] for Unbound N6-Protonated Inhibitors

	U^{elec}		U^{vdW}	
inhibitor	R^6 $inhib_{unbd}$−solv	S^6 $inhib_{unbd}$−solv	R^6 $inhib_{unbd}$−solv	S^6 $inhib_{unbd}$−solv
1a	−102.96	−112.25	−29.55	−29.21
1b	−105.83	−109.88	−28.45	−28.05
1c	−103.50	−109.96	−29.74	−27.10
1e	−99.52	−107.26	−31.48	−29.76
1f	−102.07	−104.76	−31.87	−31.85
1g	−105.68	−107.40	−28.63	−28.57
1h	−108.40	−118.68	−32.13	−26.92
1j	−103.49	−111.24	−27.53	−26.18
1k	−116.42	−125.88	−27.03	−25.98
1l	−108.16	−113.77	−26.66	−25.68
SD[b]	0.83	0.95	0.26	0.27

[a] R^6 and S^6 refer to absolute configurations of unbound N6-protonated inhibitor. [b] Average standard deviation for all inhibitors.

Table 8. Calculated Average SASA (Å^2) for Unbound N6-Protonated Inhibitors

compd	R^6 $SASA_{unbd}$	S^6 $SASA_{unbd}$
1a	557.2	561.9
1b	561.5	558.0
1c	573.1	569.7
1e	600.0	580.6
1f	578.8	582.5
1g	557.0	546.5
1h	558.6	560.6
1j	544.9	545.7
1k	537.4	550.1
1l	538.4	531.9
SD[a]	7.7	6.5

[a] Average standard deviation for all inhibitors.

Table 9. Unweighted Changes in Energy[a] and SASA from MC Simulations for Unbound N6-Protonated and Bound Neutral Inhibitors[b,c]

	R^6 inhibitor			S^6 inhibitor		
compd	ΔU^{elec} [a]	ΔU^{vdW}	ΔSASA	ΔU^{elec} [a]	ΔU^{vdW}	ΔSASA
1a	83.88	−19.27	−512.9	93.17	−19.61	−517.5
1b	86.38	−17.76	−518.0	90.43	−18.16	−514.6
1c	86.76	−21.84	−532.5	93.21	−24.47	−529.1
1e	81.12	−18.36	−537.7	90.71	−16.84	−545.4
1f	88.02	−16.82	−541.6	88.86	−20.08	−518.2
1g	83.83	−19.71	−535.8	85.55	−19.76	−525.3
1h	89.42	−19.03	−518.0	99.70	−24.24	−519.9
1j	87.25	−22.80	−522.4	95.01	−24.15	−523.3
1k	99.70	−24.37	−513.3	109.16	−25.43	−526.0
1l	92.98	−21.08	−506.0	98.59	−22.06	−499.5

[a] Not included Born correction. [b] R^6 and S^6 sections refer to the respective starting configuration of N6 in both the unbound and bound neutral simulations. [c] For these calculations, the unbound inhibitor was N6-protonated, but the bound inhibitor was neutral.

(0) systems is different, a Born correction term[9a,27] of −13.83 kcal/mol (assuming $\epsilon_r = 4$) for long-range (beyond 9 Å) electrostatic effects upon the unbound inhibitor is necessary. This correction can be applied to the LR equation (e.g., eq 1) in two slightly different fashions: either as a correction to the unbound U^{elec} (eq 4) or as an overall correction to $\Delta G_{binding}$ (eq 5). Both approaches, however, gave higher rms errors (data not shown) than the results in Tables 10 and 11 for which the Born correction was not included.

$$\Delta G_{binding} = \alpha(\langle U^{vdw}_{bound}\rangle - \langle U^{vdw}_{unbound}\rangle) + \beta(\langle U^{elec}_{bound}\rangle - \langle U^{elec}_{unbound}\rangle - \text{Born}) \quad (4)$$

$$\Delta G_{binding} = \alpha(\langle U^{vdw}_{bound}\rangle - \langle U^{vdw}_{unbound}\rangle) + \beta(\langle U^{elec}_{bound}\rangle - \langle U^{elec}_{unbound}\rangle) - \text{Born} \quad (5)$$

Uncertainty in LR Parameters and MC Results. A cross-validation analysis was used to assess the uncertainties in the LR parameters (α, β, γ, and δ). This method consists of a series of 12 (10 in the case of the protonated inhibitor studies) individual refitting calculations, each involving the omission of one of the inhibitors. The average value of the coefficients and the standard deviation for the cross-validation of each of the models are listed in Table 12. The averages are all very close to the value obtained from the complete data set, and the standard deviations are within reasonable limits.

It was noticed that large deviations in the individual cross-validation fits consistently were observed for two inhibitors in the R^6 series, **1g** and **1l**. In both of these compounds there is no substituent on the benzene ring. If these two inhibitors are excluded from consideration and the model is reparameterized, there is a substantial improvement in the accuracy of the fit. For example, the rms error for models 3 and 4 in Table 4 are 0.41 and 0.52 kcal/mol, respectively. The values of β (0.269

Table 10. Comparison of Experimental and Calculated $\Delta G_{binding}$ for Various Parameter-Fitting Models Using R^6 Unbound N6-Protonated and Bound Neutral Inhibitors

model	1	2	3	4	2a	3a	4a	
eq	1	2	2	2	3	3	3	
α	−0.390	−0.218	0.000	0.100 const	−0.227	0.000	0.100 const	
β	−0.176	0.050	0.108	0.135	0.119	0.182	0.210	exptl
γ		0.0374	0.0403	0.0417				
δ					−26.764	−28.655	−29.489	
1a	−7.25	−10.79	−11.62	−12.00	−12.45	−13.40	−13.81	−11.872
1b	−8.29	−11.19	−11.56	−11.73	−12.50	−12.94	−13.13	−11.688
1c	−6.76	−10.82	−12.10	−12.69	−11.53	−12.87	−13.46	−11.163
1e	−7.12	−12.06	−12.92	−13.32	−12.98	−13.90	−14.30	−10.600
1f	−8.94	−12.20	−12.33	−12.40	−12.52	−12.64	−12.70	−10.598
1g	−7.08	−11.56	−12.55	−13.01	−12.36	−13.40	−13.86	−10.439
1h	−8.32	−10.76	−11.23	−11.44	−11.85	−12.39	−12.62	−10.287
1j	−6.47	−10.22	−11.65	−12.30	−11.25	−12.78	−13.46	−8.521
1k	−8.05	−8.91	−9.93	−10.40	−9.42	−10.52	−11.00	−8.433
1l	−8.15	−9.69	−10.37	−10.67	−10.96	−11.74	−12.08	−7.806
rms error	2.95	1.20	1.82	2.17	1.87	2.70	3.09	

Table 11. Comparison of Experimental and Calculated $\Delta G_{binding}$ for Various Parameter-Fitting Models Using S^6 N6-Protonated Unbound and R^6 Neutral Inhibitors

model	1	2	3	4	2a	3a	4a	
eq	1	2	2	2	3	3	3	
α	−0.330	−0.124	0.000	0.100 const	−0.137	0.000	0.100 const	
β	−0.182	0.075	0.114	0.145	0.087	0.131	0.162	exptl
γ		0.0382	0.0401	0.0417				
δ					−21.337	−22.510	−23.368	
1a	−10.48	−10.33	−10.14	−9.99	−10.54	−10.34	−10.20	−11.872
1b	−10.45	−10.61	−10.34	−10.12	−10.98	−10.70	−10.50	−11.688
1c	−8.88	−10.17	−10.60	−10.95	−9.87	−10.34	−10.68	−11.163
1e	−9.54	−10.63	−10.66	−10.69	−10.85	−10.91	−10.94	−10.600
1f	−10.94	−11.93	−11.54	−11.23	−11.14	−10.66	−10.32	−10.598
1g	−9.04	−11.19	−11.33	−11.44	−11.19	−11.34	−11.45	−10.439
1h	−10.14	−9.36	−9.50	−9.60	−9.34	−9.49	−9.60	−10.287
1j	−9.31	−9.86	−10.17	−10.42	−9.76	−10.10	−10.35	−8.521
1k	−11.46	−8.74	−8.66	−8.60	−8.36	−8.25	−8.18	−8.433
1l	−10.65	−8.94	−8.81	−8.70	−9.74	−9.64	−9.56	−7.806
rms error	1.73	1.04	1.06	1.11	1.05	1.07	1.12	

and 0.297, respectively) are similar for the two methods but are significantly larger than those from the 12 inhibitor analyses (Table 4). The Lennard−Jones coefficient (model 3) is significantly smaller, $\alpha = -0.059$. The value of γ (0.0224 for both models) is less influenced by omission of **1g** and **1l**. These anomalous results for the unsubstituted TIBO derivatives are discussed more fully in the Structural Considerations section. They suggest, however, that for substituted TIBO derivatives, the U^{elec} term is highly predictive of activity.

Earlier reports[12] using the same MC method as that in the present study estimated the total statistical uncertainty in computed $\Delta G_{binding}$ to be about 0.5 kcal/mol due to noise in the MC simulations. That estimate was based on the following equation, where SU_{tot} is the total statistical uncertainty and SD is the average uncertainty (1σ) in the individual components from the MC simulations:

$$SU_{tot} = \alpha \cdot SD^{vdw} + \beta \cdot SD^{elec} + \gamma \cdot SD^{SASA}$$

From Table 2 for the neutral unbound inhibitor runs, the average uncertainties (1σ) for the U^{vdw} components are about 0.25 kcal/mol and those for U^{elec} components are about 0.50 kcal/mol. With values of 0.15 and 0.20 for α and β, respectively, these energy components would contribute a total uncertainty of about 0.15 kcal/mol. For the protonated inhibitor studies, the uncertainty is only slightly higher, 0.20 kcal/mol. The maximum uncertainty (Table 3) in the SASA values (ca. 35 Å^2) is due mainly to variation in the SASA of the bound inhibitor and would contribute an additional 0.7 kcal/mol, given a value for γ of about 0.02. Variation in the δ values, taken from the cross-validation study, is comparable at 0.7 kcal/mol. Thus the total maximum uncertainty in the $\Delta G_{binding}$ values is approximately 0.85 kcal/mol for the present study, assuming the unlikely occurrence that all of the uncertainties add together.

Structural Considerations. General. Previous crystallographic and computational reports have described the nonbonded interactions that are responsible for the favorable binding of TIBO derivatives in the NNIRT binding pocket.[5d,f,6,8] As was noted earlier, the inhibitor assumes a "butterfly" shape with two wings, and the protein forms a complementary pocket to accommodate this shape in a "shrink-wrap" fashion. The dimethylallyl moiety of the inhibitor interacts favorably with p66 amino acid residues P95, Y181, Y188, G190, and W229. The benzodiazepine ring system interacts with p66 residues K101, K103, V106, F227, H235, P236, and Y318. Located near the middle of the pocket, p66 residues L100, V179, and L234 make contact with both portions of the inhibitor.

The results of the present MC simulations show interactions with the same amino acid residues noted above. Figure 3A presents a simplified stereographic representation of a snapshot acquired during the energy-

Table 12. Cross-Validation Results for α, *β*, *γ*, and *δ* Parameters Determined from Fitting $\Delta G_{binding}$ Data[a,b]

	model						
	1	2	3	4	2a	3a	4a
				R^6 Neutral Inhibitor$_{unbd}$ Complexation Simulations			
α	0.624	−0.139		0.100 const	−0.225		0.100 const
	0.625 (0.020	*−0.138 (0.036)*			*0.222 (0.047)*		
β	0.261	0.136	0.171	0.196	0.108	0.164	0.189
	0.261 (0.038)	*0.138 (0.033)*	*0.153 (0.041)*	*0.199 (0.033)*	*0.110 (0.026)*	*0.165 (0.025)*	*0.190 (0.026)*
γ		0.0276	0.0229	0.0195			
		0.0277 (0.0013)	*0.0230 (0.0008)*	*0.0196 (0.0008)*			
δ					−15.769	−11.783	−10.013
					−15.728 (0.775)	*−11.802 (0.308)*	*−10.033 (0.328)*
				S^6 Neutral Inhibitor$_{unbd}$ Complexation Simulations			
α	0.607	−0.162		0.100 const	−0.187		0.100 const
	0.578 (0.103)	*−0.161 (0.043)*			*−0.186 (0.021)*		
β	0.243	0.092	0.133	0.159	0.118	0.159	0.180
	0.274 (0.112)	*0.093 (0.018)*	*0.130 (0.016)*	*0.159 (0.017)*	*0.119 (0.017)*	*0.159 (0.016)*	*0.181 (0.017)*
γ		0.0280	0.0224	0.0189			
		0.0280 (0.0016)	*0.0224 (0.0004)*	*0.0189 (0.0004)*			
δ					−15.232	−11.799	−9.964
				R^6 N6-Protonated Inhibitor$_{unbd}$ Complexation Simulations			
α	−0.390	−0.218		0.100 const	−0.227		0.100 const
	0.392 (0.091)	*−0.221 (0.088)*			*−0.229 (0.075)*		
β	0.176	0.050	0.108	0.135	0.119	0.182	0.210
	0.177 (0.018)	*0.050 (0.029)*	*0.108 (0.014)*	*0.135 (0.014)*	*0.121 (0.040)*	*0.186 (0.026)*	*0.213 (0.023)*
γ		0.0374	0.0403	0.0417			
		0.0376 (0.0034)	*0.0404 (0.0028)*	*0.0417 (0.0028)*			
δ					−26.764	−28.655	−29.489
					−27.376 (3.643)	*−29.032 (2.625)*	*−29.789 (2.332)*
				S^6 N6-Protonated Inhibitor$_{unbd}$ Complexation Simulations			
α	−0.330	−0.124		0.100 const	−0.137		0.100 const
	−0.334 (0.098)	*−0.133 (0.089)*			*−0.140 (0.077)*		
β	−0.182	0.075	0.114	0.145	0.087	0.131	0.162
	0.183 (0.021)	*0.072 (0.030)*	*0.114 (0.013)*	*0.146 (0.013)*	*0.087 (0.030)*	*0.132 (0.015)*	*0.165 (0.016)*
γ		0.0382	0.0401	0.0417			
		0.0381 (0.0033)	*0.0400 (0.0025)*	*0.0417 (0.0024)*			
δ					−21.337	−22.510	−23.368
					−21.380 (1.537)	*−22.661 (1.375)*	*−23.564 (1.564)*

[a] Parameters obtained using all points shown in normal text. Cross-validated values (with uncertainties) shown in italics. [b] const refers to fixed values.

averaging portion of MC simulation for the (R^6)-8-Cl TIBO/RT complex. Several of the above-named residues have been omitted from these figures for ease of viewing. To orient the reader to the general location of the binding pocket with respect to the site of polymerase activity, two members (D185 and D186) of the aspartate triad that binds the nucleoside triphosphate through two Mg^{2+} ions have been included. The DNA template and primer strands would be located above and extend to the left of W229 in the figure.

The putative original site of entry of the inhibitor into the protein and the only point of contact for the bound inhibitor with solvent is a channel bordered by p51 residue E1138 (so numbered to distinguish it from E138 in p66) and p66 residues K101 and V179. Figure 4, taken from the snapshot of the last frame in the 8-CN TIBO(O), **1k**, simulation, illustrates this last point by including the four water molecules in this channel that are within 4 Å of the inhibitor. No solvent molecules are found elsewhere in the hydrophobic binding pocket.

Hydrogen Bonding. The solvent−protein network of hydrogen bonds (H-bonds) in the vicinity of the putative entrance point (see Figure 4) is similar to that found in all of the other simulations, though the number of waters within 4 Å of the inhibitor varies from 3 to 5. Criteria for assigning the presence of a relatively strong H-bond are based on favorable geometry[28a] (angular orientation) and C═X···H−O distances of 2.40 and 1.90 Å for X = S and O, respectively.[28] A weaker H-bond was assigned using criteria where each of these distances is increased by 0.50 Å. For the analogous C═X···H−N H-bonds, an additional increment of 0.10 Å was added.[28c] The inhibitor−solvent interaction, seen in Figure 4, is present in many, but not all, of the complexes. Strong H-bonds between the thione group and a water molecule were frequently found in the 8-MeO TIBO, **1e**, and 8-CN TIBO, **1h**, complexes. Weaker H-bonds of this type were only rarely observed in the 8-F TIBO, **1b**, 8-Me TIBO, **1c**, and 8-ethynyl TIBO, **1d**, complexes and not seen at all in the remaining thione derivatives. For inhibitors bearing a keto group, only the 8-ethynyl TIBO, **1i**, and 8-CN TIBO, **1k**, complexes frequently showed a weak H-bond to solvent.

H-Bonds between the inhibitor and the backbone NH and C═O of K101 were observed in virtually all of the complexes, but the variation in these interactions may be significant. While all complexes showed a H-bond between the NH of TIBO and the backbone C═O of K101, this interaction is weakest in the most active inhibitors. By way of contrast, the existence and strength of a H-bond between the thione or keto group of the inhibitor and the backbone N−H of K101 diminish in direct proportion to the activity of the inhibitor. For example, this interaction is strong and ever present in the snapshots of 8-Cl TIBO, **1a**, while it is virtually absent in the complex with 8-H TIBO(O), **1l**.

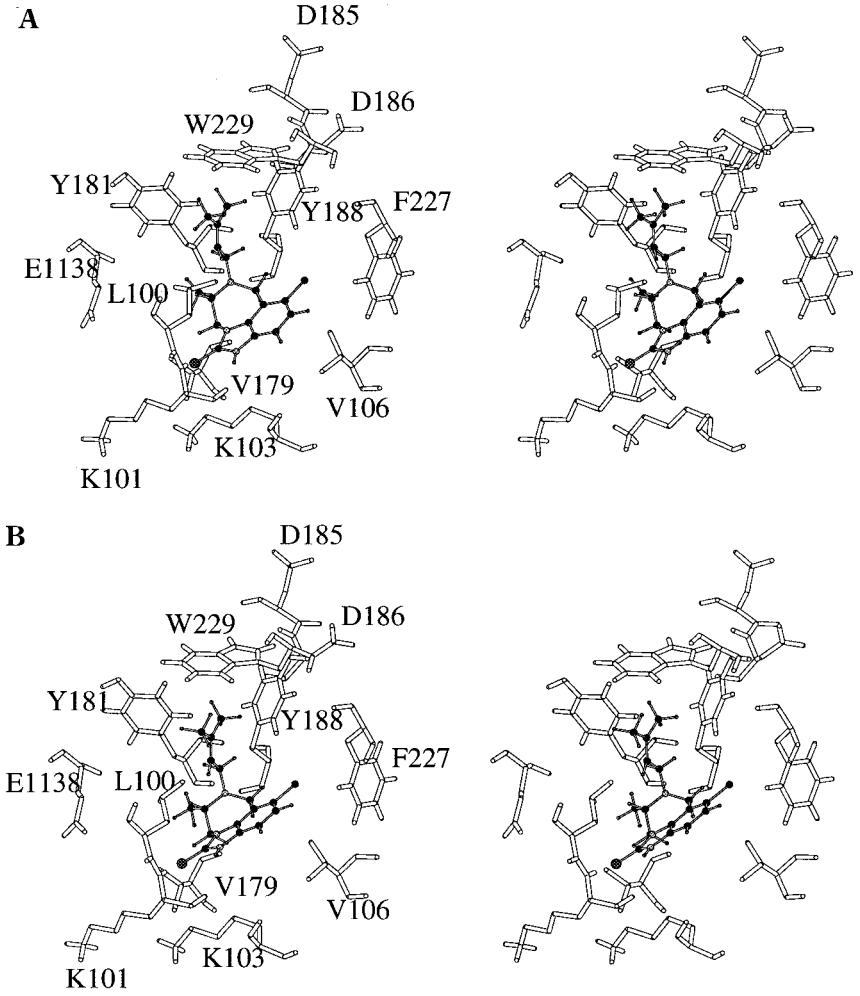

Figure 3. Stereoplots of key residues in the binding pocket from MC simulation of the 8-Cl TIBO, **1a**, complex with RT: (A) R^6 conformation of inhibitor; (B) S^6 conformation of inhibitor, illustrating inversion of N6 during simulation.

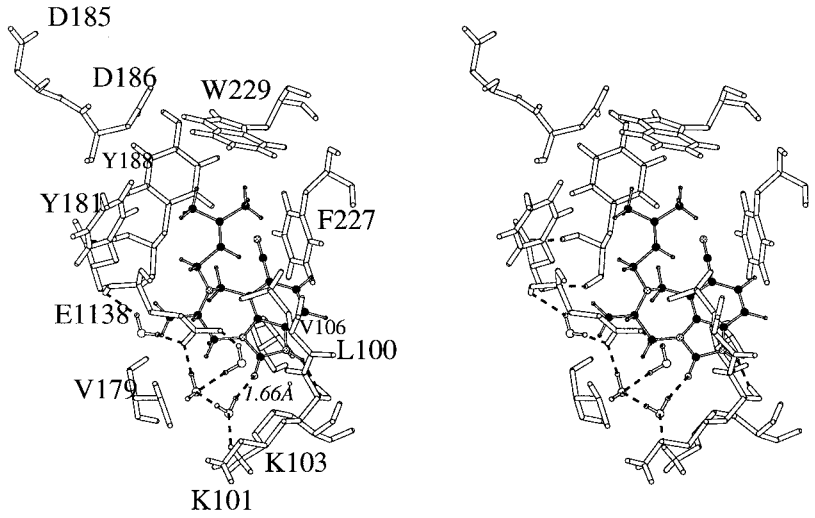

Figure 4. Stereoplot showing putative entrance to the binding pocket from MC simulation of the 8-CN TIBO(O), **1k**, complex with RT. H-Bonding network in this region between solvent, inhibitor, and protein is indicated by ⋯, and the (TIBO) C═O⋯H−O−H distance is labeled.

Thus it appears that the most active inhibitors are those that strongly hydrogen-bond to the backbone NH of K101 but do not form hydrogen bonds either to the backbone C═O of K101 or to solvent water. It is important to note, however, that this pattern may be a consequence of inhibitor−protein interactions elsewhere in the binding pocket that cause subtle shifts in the position of the inhibitor in the entrance region which in turn permit certain hydrogen-bonding interactions while excluding others.

Inhibitor Conformation and Position. During the simulations of the bound inhibitors, varying amounts of N6 inversion of the inhibitor were observed (Table 3). Returning to Figure 3, structure 3A was obtained

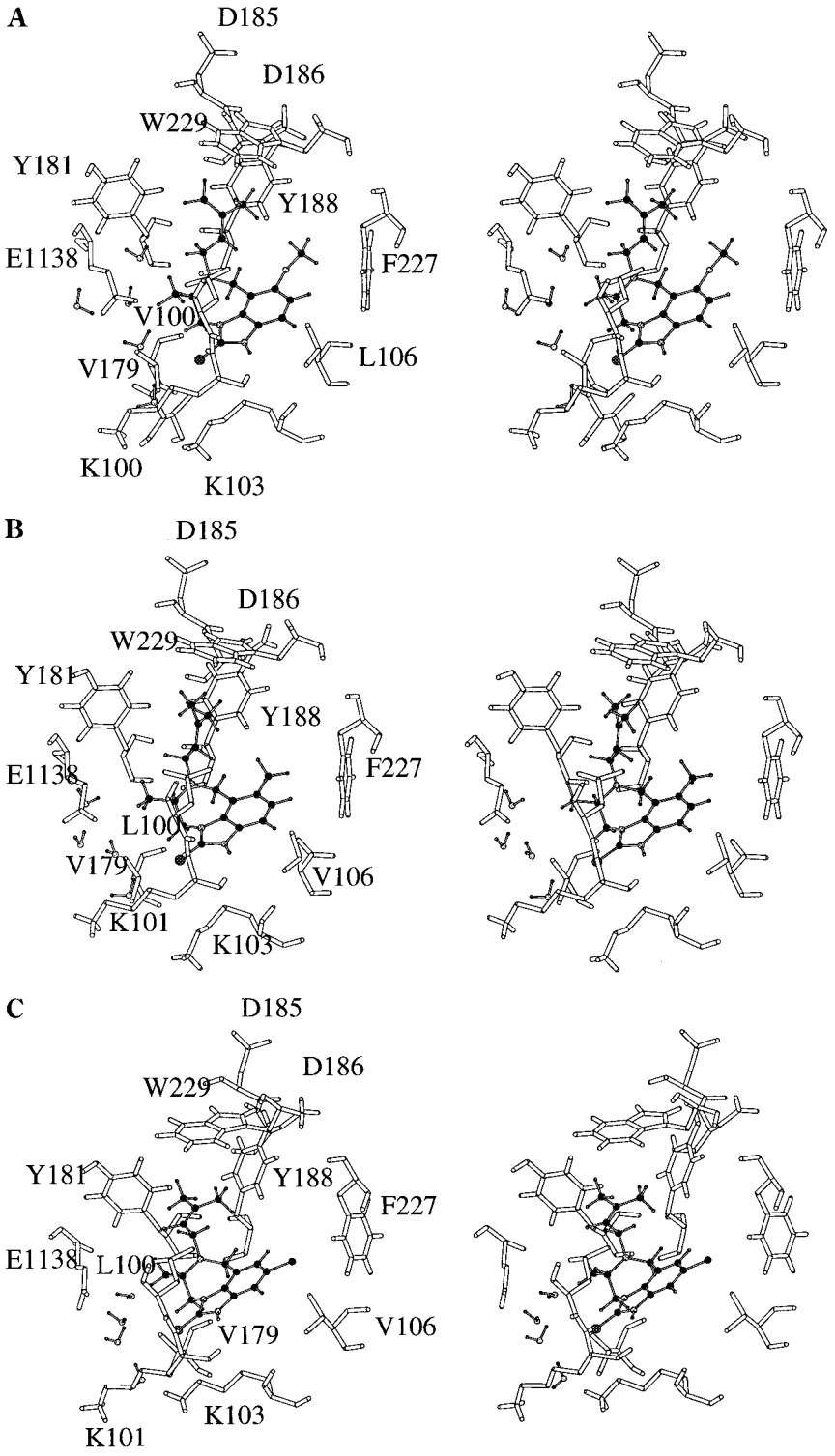

Figure 5. Stereoplots of different orientations of TIBO inhibitors in the binding pocket from MC simulation complexes with RT: (A) 8-MeO TIBO, **1e**, dimethylallyl directed toward Y188; (B) 8-Me TIBO, **1c**, dimethylallyl directed between Y181 and Y188; (C) 9-Cl TIBO, **1f**, dimethylallyl directed toward Y181.

from a snapshot about 25% of the way into the energy-averaging portions of the 8-Cl TIBO simulation and structure 3B is the final snapshot from that same simulation. These two representations demonstrate that inversion of N6 occurs during the simulation of the complex. Further, they show that the shape of the inhibitor and the orientation of the surrounding residues are very similar, irrespective of whether the inhibitor exists in the R^6 (3A) or S^6 (3B) conformation. Through much of the simulation, N6 is essentially planar, as can be seen in Figure 6. In both cases the (*E*)-methyl group of the dimethylallyl moiety makes close van der Waals contact with W229, while the (*Z*)-methyl group interacts with W229 and Y188. Only a more distant interaction is observed between the dimethylallyl group and Y181. In both conformations, the 8-chloro substituent extends into a relatively open region of the pocket surrounded by Y188, F227, and V106 and terminated in the C-Cl direction by V108 (not shown). The distance between the 8-chloro group and

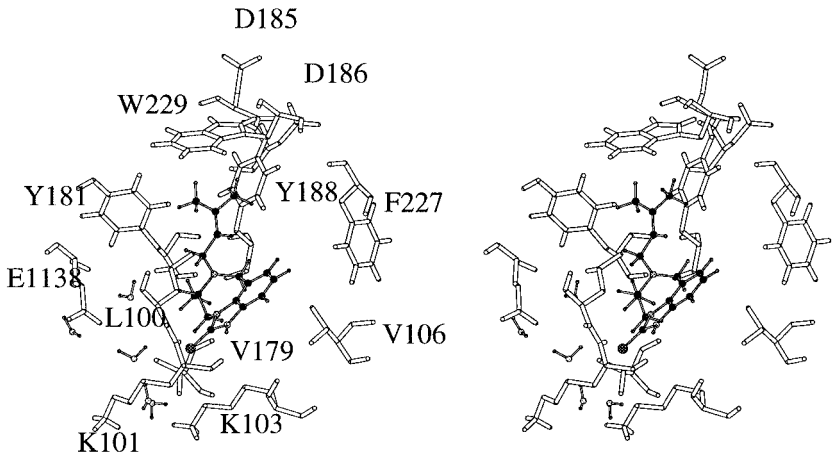

Figure 6. Stereoplot of key residues in the binding pocket from MC simulation of the 8-H TIBO, **1g**, complex with RT.

the nearest atoms (hydrogens on CG2) of V108 is 3.5 Å, allowing reasonable space to accommodate the various C8 substituents included in this study (Table 1). The 9 position on the inhibitor is, however, located in a more restricted region. This likely accounts for the poorer calculated binding energy for the 9-Cl TIBO complex, the observed lower activity of 9-Cl TIBO, and the significant alteration in the conformation of the protein in the reported crystal structure.[5f]

There appear to be several somewhat different orientations for the inhibitor in the binding pocket. Keying upon the position of the dimethylallyl group relative to the two tyrosines, Y181 and Y188, one observes three different orientations (Figure 5). In two of these positions, the plane of the dimethylallyl moiety either is oriented such that it intersects the side chain of Y181 as illustrated in Figure 5A by the 8-methoxy derivative **1e** or is oriented such that it intersects Y188, as in Figure 5C for the 9-Cl derivative **1f**. In the third position, illustrated in Figure 5B by the 8-methyl derivative **1c**, this plane takes an intermediate orientation, falling between Y181 and Y188. In the crystal structure of the 8-Cl TIBO/RT complex,[5d] the orientation is intermediate between 5B and 5C. In all three orientations, greater contact is maintained between the dimethylallyl moiety and residue Y188 as opposed to Y181. Contact between the (*E*)-methyl of the dimethylallyl group and the benzene ring of W229 is significant in all three orientations. Only in the 5B orientation, however, does the (*Z*)-methyl also make close contact with this ring of W229. Across the 5A−C series, a rotation of ∼11° (away from Y188) about the Y181 CA−CB bond indicates loss of interaction between the aryl side chain and the (*Z*)-methyl of the dimethylallyl group. Further, as the dimethylallyl reorients toward Y188, the imidazole end of the benzimidazole ring moves about 0.8 Å toward L100 and the K103 side chain follows this shift, maintaining contact with the inhibitor from below.

As might be expected, the position of each inhibitor varies throughout its respective simulation, but these variations are not the same for all of the inhibitors. For three TIBO derivatives **1a**, **1b**, and **1c**, the inhibitor visits all three of the above-noted conformations, 5A−C, in a more or less random fashion. In the case of two TIBO derivatives, **1h** and **1i**, while the initial portion of the energy averaging shows variable orientation, the dimethylallyl side chain settles into the 5A position about halfway through the run. For the remaining inhibitors, the side-chain location remains relatively stable, either in the 5A (**1e**, **1g**, **1i**, and **1k**) or in the 5C (**1d**, **1f**, and **1l**) orientation throughout the simulation. Although there is no overwhelming pattern to the preference of a given inhibitor for one or more of the orientations, it does appear that the more active inhibitors are those that assume a variety of conformations (5A−C) in the binding pocket during the simulation.

Unsubstituted TIBO Anomaly. As was noted earlier, the calculated binding energies (Tables 4 and 6) for the unsubstituted thione and keto TIBO derivatives **1g** and **1l** are much more negative (favorable) than would be expected from their observed activities. Comparison of the 8-H TIBO, **1g** , structure in Figure 6 with those of 8-Cl TIBO, **1a**, in Figure 3 reveals that the absence of a substituent at position 8 leaves a relatively open region between the inhibitor and residue F227. A similar gap exists in the analogous keto derivative **1l** complex (structure not shown). The role this gap plays in the inordinately favorable calculated binding energies for these two inhibitors is unclear. What is even more perplexing is that the MC simulation achieves a configuration which is apparently more stable than that which actually exists. One possible explanation is that, in the absence of a substituent at position 8, the inhibitor cannot induce the protein to adopt the protein backbone conformation of the 8-Cl TIBO/RT complex. It will be recalled that the simulation is based on the 8-Cl TIBO/RT crystal structure and the MCPRO program does not allow for movement of the backbone during the simulation. Unfortunately, crystallographic data for the 8-H TIBO/RT complex are not currently available. It is known that there is a substantial difference in the protein backbone conformation for the 8-Cl TIBO, **1a**, and 9-Cl TIBO, **1f**, complexes with RT.[5f] In the case of 9-Cl TIBO, however, the predicted $\Delta G_{\text{binding}}$ (Table 4) is less favorable than the observed activity. On the basis of the structure−activity trends noted above, one might venture that the actual 8-H TIBO/RT complex will show a weak H-bond to solvent, a strong NH H-bond to the K101 C═O, a weaker thione H-bond to the NH of K101, and a protein backbone conformation somewhat different from that of the 8-Cl TIBO/RT complex, but these suppositions must await crystallographic validation.

Conclusion

Monte Carlo simulations in combination with a linear response approach were used to estimate the free energies of binding for a series of 12 TIBO inhibitors of HIV-1 reverse transcriptase. Separate correlations were made for the R^6 and S^6 absolute conformations of the inhibitors, as well as for the analogous N6-monoprotonated species. Models based upon the neutral unbound inhibitors produced overall better fits to experimental values than did those using the protonated inhibitors, with only slight differences for the neutral R^6 and S^6 cases. Equation 2, a three-parameter model, gave the best overall fits when all three parameters were varied. The averaged (R^6 and S^6) rms error was approximately 0.88 kcal/mol for the observed range of 4.06 kcal/mol in inhibitor activities. The averaged values of α, β, and γ were −0.150, 0.114, and 0.0286, respectively. The negative value for the van der Waals parameter, however, is questionable on physical grounds. Omission of that component gave a very slightly worse average rms error of 0.923, with $\alpha = 0.152$ and $\beta = 0.022$. The unweighted van der Waals components are highly attractive but fail to correlate well across the series of inhibitors. Contrastingly, while the electrostatic components are all repulsive, they show a direct correlation with inhibitor activity as measured by $\Delta G_{\text{binding}}$. The role of γ, the SASA parameter, which can effectively be replaced with a negative constant, is primarily to produce an overall negative binding energy.

During the MC simulations of the unbound solvated inhibitors, the R^6 and S^6 absolute conformations do not interconvert, due to the formation of a favorable hydrogen bond to solvent. In the complex, however, interconversion of these conformations of the inhibitor is observed during the course of the simulations, a phenomenon which is apparently not observed in the crystalline state of the complex. Hydrogen bonding of the inhibitor to the backbone NH of K101, but not to the K101 C═O or solvent, seems to predict enhanced activity. Activity also appears to correlate with the ability to assume a number of different orientations of the dimethylallyl moiety with respect to residues Y181 and Y188 while continuously maintaining contact with the benzene ring of W229.

Overall, the use of a combination of Monte Carlo simulation with a linear response method shows promise as a relatively rapid means of estimating inhibitor activities. This approach should be useful in the preliminary evaluation of potential modifications to known inhibitors to enhance activity.

Acknowledgment. This research was sponsored in part by the National Cancer Institute, DHHS, under contract with ABL and by grants (R.H.S.) from the Center for Molecular Design, Janssen Research Foundation, Division of Janssen Pharmaceutica N.V., the DuPont Educational Grants Program, and the NSF-RUI, CHE-09708166. The authors wish to thank Dr. Dongchul Lim of Yale University for computational assistance and Dr. Paul J. Lewi of Center for Molecular Design, Janssen Research Foundation, for helpful discussions during the course of this work. The contents of this publication do not necessarily reflect the views or policies of the Department of Health and Human Services, nor does mention of trade names, commercial products, or organizations imply endorsement by the U.S. Government.

Supporting Information Available: Listing of nonbonded parameters and ab initio 6-31G* energies for TIBO derivatives **1a**−**1l** (4 pages). See any current masthead page for ordering information.

References

(1) Nanni, R. G.; Ding, J.; Jacobo-Molina, A.; Hughes, S. H.; Arnold, E. *Perspect. Drug Discovery Des.* **1993**, *1*, 129−150.

(2) (a) Kopp, E. B.; Miglietla, J. J.; Shrutkowski, A. G.; Shih, C. K.; Grob, P. M.; Skoog, M. T. *Nucleic Acids Res.* **1991**, *19*, 3035−3039. (b) Romero, D. L.; Bussa, M.; Tan, C. K.; Reusser, F.; Palmer, J. R.; Poppe, S. M.; Aristoff, P. A.; Downey, K. M.; So, A. G.; Resnick, L.; Tarpley, W. G. *Proc. Natl. Acad. Sci. U.S.A.* **1991**, *88*, 8806−8810.

(3) (a) Esnouf, R.; Ren, J.; Ross, C.; Jones, Y.; Stammers, D.; Stuart, D. *Struct. Biol.* **1995**, *2*, 303−308. (b) Rodgers, D. W.; Gamblin, S. J.; Harris, B. A.; Ray, S.; Culp, J. S.; Hellmig, B.; Woolf, D. J.; Debouck, C.; Harrison, S. C. *Proc. Natl. Acad. Sci. U.S.A.* **1995**, *92*, 1222−1226. (c) Patel, P.; Jacobo-Molina, A.; Ding, J.; Tantillo, T.; Clark, A. D.; Raag, R.; Nanni, R. G.; Hughes, S. H.; Arnold, E. *Biochemistry* **1995**, *34*, 5351−5363.

(4) Jacobo-Molina, A.; Ding, J.; Nanni, R. G.; Clark, A. D., Jr.; Lu, X.; Tantillo, C.; Williams, R. L.; Kamer, G.; Ferris, A. L.; Clark, P.; Hizi, A.; Hughes, S. H.; Arnold, E. *Proc. Natl. Acad. Sci. U.S.A.* **1993**, *90*, 6320−6324.

(5) (a) Kohlstaedt, L. A.; Wang, J.; Friedman, J. M.; Rice, P. A.; Steitz, T. A. *Science* **1992**, *256*, 1783−1790. (b) Jager, J.; Smerdon, S.; Wang, J.; Boisvert, D. C.; Steitz, T. A. *Structure* **1994**, *2*, 869−876. (c) Smerdon, S. J.; Jager, J.; Wang, J.; Kohlstaedt, L. A.; Chirino, A. J.; Friedman, J. M.; Rice, P. A.; Steitz, T. A. *Proc. Natl. Acad. Sci. U.S.A.* **1994**, *91*, 3911−3915. (d) Ding, J.; Das, K.; Moereels, H.; Koymans, L.; Andries, K.; Janssen, P. A. J.; Hughes, S. H.; Arnold, E. *Nature Struct. Biol.* **1995**, *2*, 407−415. (e) Ding, J.; Das, K.; Tantillo, C.; Zhang, W.; Clark, A. D., Jr.; Jessen, S.; Lu, X.; Hsiou, Y.; Jacobo-Molina, A.; Andries, K.; Pauwels, R.; Moereels, H.; Koymans, L.; Janssen, P. A. J.; Smith, R. H., Jr.; Koepke, M. B. K.; Michejda, C. J.; Hughes, S. H.; Arnold, E. *Structure* **1995**, *3*, 365−379. (f) Das, K.; Ding, J.; Hsiou, Y.; Clark, A. D.; Moereels, H.; Koymans, L.; Andries, K.; Pauwels, R.; Janssen, P. A. J.; Boyer, P. L.; Clark, P.; Smith, R. H., Jr.; Kroeger Smith, M. B.; Michejda, C. J.; Hughes, S. H.; Arnold, E. *J. Mol. Biol.* **1996**, *264*, 1085−1100.

(6) Smith, M. B. K.; Rouzer, C. A.; Taneyhill, L. A.; Smith, N. A.; Hughes, S. H.; Boyer, P. L.; Janssen, P. A. J.; Moereels, H.; Koymans, L.; Arnold, E.; Ding, J.; Das, K.; Zhang, W.; Michejda, C. J.; Smith, R. H., Jr. *Protein Sci.* **1995**, *4*, 2203−2222.

(7) (a) Spence, R. A.; Kati, W. M.; Anderson, K. S.; Johnson, K. A. *Science* **1995**, *267*, 988−993. (b) Spence, R. A.; Anderson, K. S.; Johnson, K. A. *Biochemistry* **1996**, *35*, 1054−1063.

(8) (a) Smith, R. H., Jr.; Michejda, C. J.; Hughes, S. H.; Arnold, E.; Janssen, P. A. J.; Smith, M. B. K. *THEOCHEM (J. Mol. Struct.)* **1998**, *423*, 67−77. (b) Smith, M. B. K.; Michejda, C. J.; Hughes, S. H.; Boyer, P. L.; Janssen, P. A. J.; Andries, K.; Buckheit, R. W., Jr.; Smith, R. H., Jr. *Protein Eng.* **1997**, *10*, 1379−1383.

(9) (a) Aqvist, J.; Medina, C.; Samuelsson, J.-E. *Protein Eng.* **1994**, *7*, 385−391. (b) Hansson, T.; Aqvist, J. *Protein Eng.* **1995**, *8*, 1137−1144. (c) Aqvist, J.; Hansson, T. *J. Phys. Chem.* **1996**, *100*, 9512−9521. (d) Aqvist, J. *J. Comput. Chem.* **1996**, *17*, 1587−1597. (e) Hulten, J.; Bonham, N. M.; Nillroth, U.; Hansson, T.; Zuccarello, G.; Bouzide, A.; Aqvist, J.; Classon, B.; Danielson, U. H.; Karlen, A.; Kvarnstrom, I.; Samuelsson, B.; Hallberg, A. *J. Med. Chem.* **1997**, *40*, 885−897.

(10) Carlson, H. A.; Jorgensen, W. L. *J. Phys. Chem.* **1995**, *99*, 10667−10673.

(11) Hansson, T.; Marelius, J. Aqvist, J. *J. Comput.-Aided Mol. Des.* **1998**, *12*, 27−35.

(12) Jones-Hertzog, D. K.; Jorgensen, W. L. *J. Med. Chem.* **1997**, *40*, 1539−1549.

(13) McDonald, N. A.; Carlson, H. A.; Jorgensen, W. L. *J. Phys. Org. Chem.* **1997**, *10*, 563−576.

(14) Liaw, Y.-C.; Gao, Y.-G.; Robinson, H.; Wang, A. H.-J. *J. Am. Chem. Soc.* **1991**, *113*, 1857−1859.

(15) Boessenkool, I. K.; Boeyens, J. A. *J. Cryst. Mol. Struct.* **1980**, *10*, 11−18.

(16) Frisch, M. J.; Trucks, G. W.; Head-Gordon, M.; Gill, P. M. W.; Wong, M. W.; Foresman, J. B.; Johnson, B. G.; Schelgal, H. B.; Robb, M. A.; Replogle, E. S.; Gomperts, R.; Andres, J. L.; Raghavachari, K.; Binkley, J. S.; Gonzalez, C.; Martin, R. L.; Fox, D. L.; Defrees, D. J.; Baker, J.; Stewart, J. J. P.; Pople, J. A. Gaussian94; Gaussian, Inc.: Pittsburgh, PA, 1994.

(17) A. Jacobs, P. J. Lewi, and P. A. J. Janssen, Analytical Development Department, Janssen Research Foundation, private communication.

(18) Jorgensen, W. L. MCPRO, version 1.5; Yale University: New Haven, CT, 1996.
(19) Jorgensen, W. L.; Maxwell, D. S.; Tirado-Rives, J. *J. Am. Chem. Soc.* **1996**, *118*, 11225−11236.
(20) Jorgensen, W. L. BOSS, version 3.6; Yale University: New Haven, CT, 1995.
(21) (a) Carlson, H. A.; Nguyen, M.; Orozco, M.; Jorgensen, W. L. *J. Comput. Chem.* **1993**, *14*, 1240−1249. (b) Breneman, C. M.; Wiberg, K. B. *J. Comput. Chem.* **1990**, *11*, 361−373.
(22) Skell, J. M.; Pearlman, R. S. SAVOL2; University of Texas: Austin, TX, 1988.
(23) Jorgensen, W. L.; Tirado-Rives, J. *J. Am. Chem. Soc.* **1988**, *110*, 1657−1671.
(24) Ho, W.; Kukla, M. J.; Breslin, H. J.; Ludovici, D. W.; Grous, P. P.; Diamond, C. J.; Miranda, M.; Rodgers, J. D.; Ho, C. Y.; De Clercq, E.; Pauwels, R.; Andries, K.; Janssen, M. A. C.; Janssen, P. A. J. *J. Med. Chem.* **1995**, *38*, 794−802.
(25) Cheng, Y.; Prusoff, W. H. *Biochem. Pharmacol.* **1973**, *22*, 3099−3108.
(26) Hall, H. K., Jr. *J. Am. Chem. Soc.* **1957**, *79*, 5441−5444.
(27) Straatsma, T. P.; Berendsen, H. J. C. *J. Chem. Phys.* **1988**, *89*, 5876−5886.
(28) (a) Taylor, R.; Kennard, O.; Versichel, W. *J. Am. Chem. Soc.* **1983**, *105*, 5761−5766. (b) Lautie, A.; Novak, A. *Chem. Phys. Lett.* **1980**, *71*, 290−293. (c) Vedani, A.; Dunitz, J. D. *J. Am. Chem. Soc.* **1985**, *107*, 7653−7658.

JM9804174